



**HAL**  
open science

# Adaptive Disturbance Observer for Trajectory Tracking of Underwater Vehicles

Jesus Guerrero, Jorge Antonio Torres Muñoz, Vincent Creuze, Ahmed Chemori

► **To cite this version:**

Jesus Guerrero, Jorge Antonio Torres Muñoz, Vincent Creuze, Ahmed Chemori. Adaptive Disturbance Observer for Trajectory Tracking of Underwater Vehicles. *Ocean Engineering*, 2020, 200, pp.#107080. 10.1016/j.oceaneng.2020.107080 . lirmm-02484279

**HAL Id: lirmm-02484279**

**<https://hal-lirmm.ccsd.cnrs.fr/lirmm-02484279v1>**

Submitted on 19 Feb 2020

**HAL** is a multi-disciplinary open access archive for the deposit and dissemination of scientific research documents, whether they are published or not. The documents may come from teaching and research institutions in France or abroad, or from public or private research centers.

L'archive ouverte pluridisciplinaire **HAL**, est destinée au dépôt et à la diffusion de documents scientifiques de niveau recherche, publiés ou non, émanant des établissements d'enseignement et de recherche français ou étrangers, des laboratoires publics ou privés.

# Adaptive Disturbance Observer for Trajectory Tracking of Underwater Vehicles

J. Guerrero<sup>a</sup>, J. Torres<sup>a</sup>, V. Creuze<sup>b</sup>, A. Chemori<sup>b</sup>

<sup>a</sup>*Center for Research and Advanced Studies of the National Polytechnic Institute (CINVESTAV), Automatic Control Department, Mexico City, MX, 07360, (e-mail: {jguerrero, jtorres}@ctrl.cinvestav.mx).*

<sup>b</sup>*LIRMM, Univ. Montpellier, CNRS, Montpellier, France (e-mail: {vincent.creuze, ahmed.chemori}@lirmm.fr).*

---

## Abstract

Complex and highly coupled dynamics, time-variance, unpredictable disturbances and lack of knowledge of hydrodynamic parameters, complicate the control of underwater vehicles. This paper deals with the adaptive disturbance observer design for the robust trajectory tracking problem for underwater vehicles in presence of unknown external disturbances and parametric uncertainties. First, the dynamics of the vehicle is transformed into the so-called regular form. Then, based on the Extended State Observer technique and High Order Sliding Modes Control, a disturbance observer is proposed. Furthermore, the gains of the observer are automatically adjusted by the introduction of an adaption law. The stability of the whole controller/observer scheme is proven using Lyapunov's arguments. The adaptive disturbance observer aims to improve the Backstepping and nonlinear PD controllers. Real-Time experiments demonstrate the effectiveness of the proposed algorithm for the trajectory tracking task under several scenarios.

*Keywords:* Sliding Mode Control, Backstepping, PD, Autonomous Underwater Vehicles, Adaptive Control

---

## 1. Introduction

2 The Remotely Operated Vehicles (ROVs) and Autonomous Underwaters  
3 Vehicles (AUVs) have been an invaluable tool for research marine environ-  
4 ment. These two classes of underwater vehicles has proven their value in  
5 a wide range of applications, such as inspection, exploration, oceanography,

6 biology, and so on. In some applications, the vehicle's autonomy plays a  
7 fundamental role in the success of the mission. Thus, to provide autonomy  
8 to underwater vehicles, there are three main tasks to perform, namely: 1)  
9 Station keeping, which refers to maintaining the vehicle to constant position  
10 and attitude; 2) Path following which is the task where the vehicle follows a  
11 spatial reference; and 3) Trajectory tracking, which means that the vehicle  
12 follows a time varying trajectory. In this paper, we focus on the first and  
13 third cases.

14 The design of a trajectory tracking controller for an underwater vehicle  
15 is not trivial. The control of underwater vehicles is challenging due to the  
16 non-linearity, time-variance, random external disturbances, such as the envi-  
17 ronmental force generated by the sea current fluctuation, and the difficulty  
18 in accurately modeling hydrodynamic effects [1].

19 Several strategies have been proposed to control underwater vehicles, such  
20 as Proportional-Derivative (PD) control [2, 3], Proportional Integral Deriva-  
21 tive (PID) control [4, 5],  $H_2$  and  $H_\infty$  control [6], Optimal Control [7], to name  
22 a few. Moreover, many controllers were designed employing the linearized  
23 model of underwater vehicles, considering strong restrictive assumptions to  
24 simplify the mathematical description, resulting sometimes in low robustness  
25 to both external disturbances and model uncertainties. This is the reason  
26 why many researchers concentrated their interests in developing robust con-  
27 trollers for underwater vehicles.

28 The Sliding Mode Control (SMC) is a robust technique, which allows  
29 controlling the vehicle despite external disturbances and parameters uncer-  
30 tainties. For example, a second order sliding mode controller for trajectory  
31 tracking task for an underwater vehicle is proposed in [8]. In order to mini-  
32 mize the energy consumption of the controller, a Super-Twisting SMC with  
33 region concept is proposed in [9]. However, the main drawback of the SMC is  
34 the chattering effect induced by the signum function. Although other func-  
35 tions can replace the signum function [10], it constrains the sliding systems  
36 trajectories, not to the sliding surface but to its vicinity, thus partly losing  
37 the robustness to the disturbances [11].

38 Backstepping Control (BSC) is another popular technique, sometimes  
39 used to control underwater vehicles. The BSC technique offers a system-  
40 atic procedure to construct the Lyapunov functions and related stabilizing  
41 feedback control laws recursively [12]. For example, a bioinspired filtered  
42 Backstepping tracking control for the kinematic model of an underwater ve-  
43 hicle is proposed in [13]. In [14] an error-based block BSC for the trajectory

44 tracking of a submarine is proposed. However, the drawback of the BSC is  
45 that it requires perfect cancellation of the robot's nonlinear dynamics, which  
46 means that the exact knowledge of this latter is needed.

47 PD and PID controllers are popular techniques used to control the posi-  
48 tion and attitude of underwater vehicles due to their simple design and good  
49 performance. However, it is well-known that the performance of the PD/PID  
50 controller is degraded when the plant is highly nonlinear or time-varying. To  
51 overcome these drawbacks, the PD/PID controllers are improved adopting  
52 strategies based on auto-adjustable [15], saturated [16], adaptive [17], or  
53 nonlinear functions [18, 19]. For instance, a nonlinear PID for the trajec-  
54 tory tracking of an AUV is proposed in Guerrero et al. [19]. In this work, a  
55 PID was saturated by a whole set of nonlinear functions in order to provide  
56 robustness towards external disturbances and parametric uncertainties. In  
57 general, PD and PID improved controllers can preserve easy design and gain  
58 robustness towards external disturbance, as one can see on the results of the  
59 above cited papers.

60 The disturbance observation focuses on controller improvement through  
61 counteracting of the disturbances. For example, the Extended State Ob-  
62 server (ESO) methodology is applied to an AUV trajectory tracking in [20].  
63 In this work, the authors propose an adaptive ESO algorithm to estimate  
64 the unknown submarine velocity, parametric uncertainties and external dis-  
65 turbances for the full six Degrees of Freedom (DoF) of the system. Then,  
66 an Integral Sliding Mode Control (ISMC) is designed and includes the dis-  
67 turbance estimation made by the ESO. Based on real-time experiments, the  
68 authors show the improvement of the ISMC and compare the proposed al-  
69 gorithm with the classical PD controller. Nonetheless, the proposed control  
70 scheme needs the adjustment of many controller gains, which can be time-  
71 consuming. Also, the control law uses the signum function, which causes  
72 chattering, as can be seen on the reported control input graphs. Finally, al-  
73 though the algorithm was designed to compensate parametric uncertainties,  
74 experiments about robustness against parameter changes are not shown.

75 In this paper, we develop an adaptive disturbance observer based on  
76 the Generalized Super-Twisting Algorithm (GSTA) [21] through the ESO  
77 technique in order to improve robustness to both external disturbances and  
78 model uncertainties. For example, based on the real-time experiments shown  
79 in work [14], the proposed BSC shows a constant offset between the vehicle  
80 and the desired trajectory. Similarly, in the experiments that were carried  
81 out with a nonlinear PD (NLPD) control law, in the study [18], we can

82 observe a constant error in steady-state behavior in the depth tracking tests  
 83 when parametric uncertainties are considered. In this sense, the developed  
 84 disturbance observer is introduced into BSC and NLPD control laws, in order  
 85 to counteract the effects of the external disturbances and the parametric  
 86 uncertainties.

87 The main contributions of this paper are as follows:

- 88 1. An Adaptive disturbance observer based on High Order Sliding Mode  
 89 Controllers and Extended State Observer is developed to estimate and  
 90 compensate the effects of external disturbances and parameters uncer-  
 91 tainties during trajectory tracking for an underwater vehicle. Moreover,  
 92 the stability analysis of the whole scheme observer/controller is proven  
 93 by Lyapunov's arguments.
- 94 2. The adaptive GSTA-ESO extends our previous results (see Guerrero  
 95 et al. [22]) introducing adaption laws to update the observer's gains,  
 96 then relaxing the requirement of knowing the upper bound of pertur-  
 97 bations.
- 98 3. The GSTA-ESO improves the BSC and NLPD controllers performances  
 99 shown in [14] and [18], respectively.
- 100 4. The effectiveness of the proposed adaptive observer is validated through  
 101 real-time experiments.

102 The rest of the paper is organized as follows: a brief description of the  
 103 dynamics of an underwater vehicle is given in Section 2. BSC and NLPD  
 104 enhancement with the adaptive disturbance observer technique are described  
 105 in Section 3. The real-time experimental results for two DoF trajectory  
 106 tracking are presented and analyzed in Section 4. Finally, some concluding  
 107 remarks are delineated in Section 5.

## 108 2. Dynamic Model

109 The mathematical model is described with respect to an earth-fixed frame  
 110  $(x_I, y_I, z_I)$ , and a body-fixed reference frame  $(x_b, y_b, z_b)$  as shown in Figure 1.

The matrix of spatial transformation between the inertial frame and the  
 frame of the rigid body can be defined through the transformation of the  
 Euler angles,  $J(\eta)$ , and the following equation:

$$\dot{\eta} = J(\eta)\nu \tag{1}$$

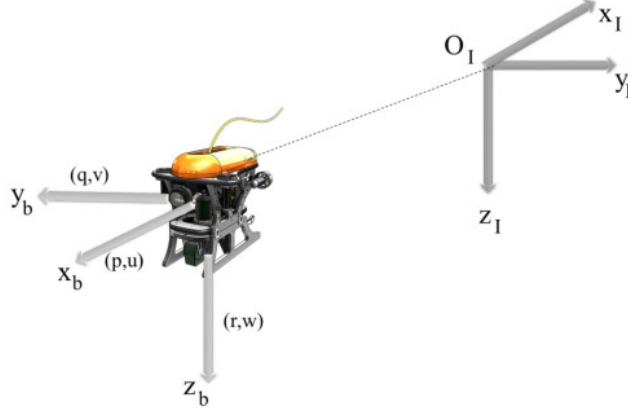


Figure 1: *Leonard* underwater vehicle reference frames. The earth-fixed frame is denoted  $(O_I, x_I, y_I, z_I)$  and the body-fixed frame is denoted  $(O_b, x_b, y_b, z_b)$ .

where  $\nu = [u, v, w, p, q, r]^T$  is the vector of velocity in the body-fixed frame and  $\eta = [x, y, z, \phi, \theta, \psi]^T$  represents the vector of position and orientation in the earth-fixed frame. Moreover, the SNAME notation [23] is usually employed to describe the mathematical model of the underwater vehicles, which can be written as follows [4, 24, 5, 25]:

$$M(\nu)\dot{\nu} + C(\nu)\nu + D(\nu)\nu + g(\eta) = \tau + w_e(t) \quad (2)$$

111 where  $M(\nu) \in \mathbb{R}^{6 \times 6}$  is the matrix of inertia (including the effects of added  
 112 mass),  $C(\nu) \in \mathbb{R}^{6 \times 6}$  is the Coriolis-centripetal matrix,  $D(\nu) \in \mathbb{R}^{6 \times 6}$  repre-  
 113 sents the hydrodynamic damping matrix,  $g(\eta) \in \mathbb{R}^6$  is the vector of gravita-  
 114 tional/buoyancy forces and moments. Finally,  $\tau \in \mathbb{R}^6$  is the control vector  
 115 acting on the underwater vehicle, and  $w_e(t) \in \mathbb{R}^6$  represents the vector of  
 116 external disturbances.

By applying the velocity transformation mapping given by Eq. (1) to Eq. (2), it is possible to express the dynamics in the earth-fixed frame as follows (see [14, 22] for more details):

$$\underbrace{M_\eta(\eta)\ddot{\eta} + C_\eta(\nu, \eta)\dot{\eta} + D_\eta(\nu, \eta)\dot{\eta} + g_\eta(\eta)}_{f(\eta, \nu)} = \tau_\eta + w_\eta(t) \quad (3)$$

where  $f(\eta, \nu)$  is the system dynamics. As highlighted by the work [4, 24], the elements of the matrices of the dynamic model (3) depend of a large set

of parameters, difficult to estimate [26]. For this reason, it is common to introduce assumptions to reduce the number of parameters. From equation (3), the system dynamics  $f(\eta, \nu)$  can be written as the sum of the estimated dynamics  $\hat{f}(\eta, \nu)$  and the unknown dynamics  $\tilde{f}(\eta, \nu)$ , as follows:

$$f(\eta, \nu) = \hat{f}(\eta, \nu) + \tilde{f}(\eta, \nu) \quad (4)$$

where:

$$\hat{f}(\eta, \nu) = \hat{M}_\eta(\eta)\ddot{\eta} + \hat{C}_\eta(\nu, \eta)\dot{\eta} + \hat{D}_\eta(\nu, \eta)\dot{\eta} + \hat{g}_\eta(\eta) \quad (5)$$

$$\tilde{f}(\eta, \nu) = \tilde{M}_\eta(\eta)\ddot{\eta} + \tilde{C}_\eta(\nu, \eta)\dot{\eta} + \tilde{D}_\eta(\nu, \eta)\dot{\eta} + \tilde{g}_\eta(\eta) \quad (6)$$

117 here the matrices of the unknown dynamics vector  $\tilde{f}(\eta, \nu)$  are defined as  
 118  $\tilde{M}_\eta = M_\eta - \hat{M}_\eta$ ,  $\tilde{C}_\eta = C_\eta - \hat{C}_\eta$ ,  $\tilde{D}_\eta = D_\eta - \hat{D}_\eta$  and  $\tilde{g}_\eta = g_\eta - \hat{g}_\eta$ .

Finally, the mathematical model of the underwater vehicle can be expressed with respect to known parameters by introducing the relation (4) into the dynamic system (3), which leads to

$$\hat{M}_\eta(\eta)\ddot{\eta} + \hat{C}_\eta(\nu, \eta)\dot{\eta} + \hat{D}_\eta(\nu, \eta)\dot{\eta} + \hat{g}_\eta(\eta) = \tau_\eta + \bar{d}(t) \quad (7)$$

119 where the lumped unknown disturbance vector is defined as  $\bar{d}(t) = w_\eta(t) -$   
 120  $\tilde{f}(\eta, \nu)$ . It is worth to note that the disturbance vector  $\bar{d}(t)$  contains the  
 121 effects of the external disturbance and the unknown dynamics as well.

### 122 **3. Adaptive Disturbance Observer and Trajectory Tracking Con-** 123 **troller Design**

124 In this section, a new adaptive disturbance observer is introduced. This  
 125 observer is based on the Extended State Observer technique which has been  
 126 proposed originally in [27, 28]. The ESO method is applied to integral chain  
 127 systems. The main idea behind the ESO technique is to design a state ob-  
 128 server for a new augmented system, which considers the external disturbance  
 129 term as an additional state. Then, the estimation made by the observer will  
 130 provide information about the system's states and the external disturbance  
 131 as well. The main drawback of this technique is that the bound of the ex-  
 132 ternal disturbance needs to be known precisely in order to obtain a proper  
 133 tuning of the observer's gains. Based on this issue, in the study [29], we pro-  
 134 posed a GSTA-ESO based on High Order Sliding Modes theory. The main  
 135 advantage of the proposed method is that the estimation of the disturbance

136 is made in finite time. The effectiveness of the GSTA-ESO is demonstrated  
 137 through real-time experiments. The experiments show the improvement of  
 138 the NLPD nominal design towards parametric uncertainties and external dis-  
 139 turbances as well. In theory, the observer of the proposed scheme has three  
 140 gains to tune, directly related to the upper bound of the disturbance. In  
 141 this manuscript, we have extended the results shown in our previous work,  
 142 introducing adaption laws to update the observer's gains depending on the  
 143 disturbance evolution. It means that the controller will be capable of re-  
 144 jecting bounded time-varying disturbances even if the upper bound of the  
 145 perturbation is not known.

### 146 3.1. Adaptive Disturbance Observer Design

First, from the vehicle's dynamics described by Eq. (7), we introduce the following state variables:

$$\zeta_1(t) = \eta(t) \quad ; \zeta_2(t) = \dot{\eta}(t) \quad (8)$$

Then, the mathematical model, (7), can be rewritten into the so-called regular form as follows:

$$\begin{aligned} \dot{\zeta}_1(t) &= \zeta_2(t) \\ \dot{\zeta}_2(t) &= \bar{F}(\zeta) + G(\zeta)\tau_\eta + d(t) \end{aligned} \quad (9)$$

where:

$$\begin{aligned} \bar{F}(\zeta) &= -\hat{M}_n(\eta)^{-1} \left[ \hat{C}_n(\nu, \eta)\dot{\eta} + \hat{D}_\eta(\nu, \eta)\dot{\eta} + \hat{g}_\eta(\eta) \right] \\ G(\zeta) &= \hat{M}_n(\eta)^{-1} \\ d(t) &= \hat{M}_\eta(\eta)^{-1}\bar{d}(t) \end{aligned}$$

147 Before proposing the adaptive disturbance observer, we need to introduce  
 148 the following assumptions:

149 **Assumption 1.** *The pitch angle is smaller than  $\pi/2$ , i.e.,  $|\theta| < \pi/2$ .*

150 **Assumption 2.** *The external disturbance  $d(t)$  is a Lipschitz continuous sig-  
 151 nal, but its upper bound is not necessarily known.*

According to Assumption 1, the inverse of the matrix  $J(\eta)$  exists. Also, according to Assumption 2, the time derivative of the lumped external disturbance terms  $d(t)$  exists almost everywhere and it is bounded:

$$|\dot{d}_i(t)| \leq L_i, \quad i = \overline{1, 6} \quad (10)$$

152 In this work, we assume that the waves and currents fulfill Assumption 2.

The first step of the design of the adaptive disturbance observer is to introduce the next auxiliary variable  $\sigma(t)$  defined as:

$$\sigma(t) = \zeta_2(t) + \Lambda \zeta_1(t) \quad (11)$$

153 where  $\sigma(t) := [\sigma_1, \sigma_2, \dots, \sigma_6]^T$  and  $\Lambda = \text{diag}(\lambda_1, \lambda_2, \dots, \lambda_6)$  is a diagonal,  
154 and positive definite matrix.

Computing the time derivative of (11) leads to:

$$\dot{\sigma}(t) = F(\zeta) + G(\zeta)\tau_\eta + d(t) \quad (12)$$

155 with  $F(\zeta) = \overline{F}(\zeta) + \Lambda \dot{\zeta}_1(t)$ .

The second step is to consider the total disturbance  $d(t)$  in Eq. (12) as an extended state  $\chi(t)$  as follows:

$$\begin{aligned} \dot{\sigma}(t) &= F(\zeta) + G(\zeta)\tau_\eta + \chi(t) \\ \dot{\chi}(t) &= h(t) \end{aligned} \quad (13)$$

156 where  $h(t)$  is the time derivative of the total disturbance  $d(t)$ .

157 **Remark 1.** *It is worth to note that the time derivative of the disturbance,*  
158  *$h(t)$ , is used to design the disturbance observer only. This parameter will be*  
159 *estimated by the adaptive algorithm.*

Finally, we propose a new disturbance observer which is constructed as follows:

$$\begin{aligned} \tilde{\sigma}(t) &= \hat{\sigma}(t) - \sigma(t) \\ \tilde{\chi}(t) &= \hat{\chi}(t) - \chi(t) \\ \dot{\tilde{\sigma}} &= F(\zeta) + G(\zeta)\tau_\eta - K_1 \Phi_1(\tilde{\sigma}) + \hat{\chi}(t) \\ \dot{\tilde{\chi}} &= -K_2 \Phi_2(\tilde{\sigma}) \end{aligned} \quad (14)$$

where  $\tilde{\sigma}(t)$  and  $\tilde{\chi}(t)$  are respectively the estimation error of the ESO and the estimation error of the disturbance  $\chi(t)$ .  $\hat{\sigma}(t)$  and  $\hat{\chi}(t)$  are the observer

internal states.  $\hat{\sigma}(t)$  and  $\hat{\chi}(t)$  are the dynamics of the observer internal states and the vectors  $\Phi_1(\tilde{\sigma}) = [\phi_{11}, \phi_{12}, \dots, \phi_{16}]^T$  and  $\Phi_2(\tilde{\sigma}) = [\phi_{21}, \phi_{22}, \dots, \phi_{26}]^T$  and each element of the mentioned vectors is given by:

$$\begin{aligned}\phi_{1i}(\tilde{\sigma}_i) &= \mu_{1i}|\tilde{\sigma}_i|^{1/2}\text{sgn}(\tilde{\sigma}_i) + \mu_{2i}\tilde{\sigma}_i \\ \phi_{2i}(\tilde{\sigma}_i) &= \frac{1}{2}\mu_{1i}^2\text{sgn}(\tilde{\sigma}_i) + \frac{3}{2}\mu_{1i}\mu_{2i}|\tilde{\sigma}_i|^{1/2}\text{sgn}(\tilde{\sigma}_i) + \mu_{2i}^2\tilde{\sigma}_i\end{aligned}$$

where  $\mu_{1i}, \mu_{2i} \geq 0$  with  $i = \overline{1, 6}$ ,  $K_1 = \text{diag}(k_{11}, k_{12}, \dots, k_{16})$  and  $K_2 = \text{diag}(k_{21}, k_{22}, \dots, k_{26})$  are the observer gains which are definite positive matrices. Moreover, if each element of the observer gain matrices is selected as follows:

$$k_{1i}(t) = \begin{cases} \omega_i \sqrt{\frac{\varsigma_i}{2}} & \text{if } \tilde{\sigma} \neq 0 \\ 0 & \text{if } \tilde{\sigma} = 0 \end{cases} \quad (15)$$

$$k_{2i}(t) = 2\epsilon_i k_{1i}(t) + \beta_i + 4\epsilon_i^2 \quad (16)$$

160 where  $\omega_i, \varsigma_i, \beta_i$  and  $\epsilon_i$  are arbitrary positive constants, with  $i = \overline{1, 6}$ . Then,  
 161 for any initial condition  $\tilde{\sigma}_i(0)$  and  $\tilde{\chi}_i(0)$ , the variables  $\tilde{\sigma}_i$  and  $\tilde{\chi}_i$  will tend to  
 162 zero in a finite time as is stated in the next.

163 **Theorem 1.** *Consider the perturbed augmented system (13). The proposed*  
 164 *AGSTA-ESO (14) ensures that the observer error dynamics converges to zero*  
 165 *in finite time if the gains  $K_1$  and  $K_2$  are definite positive matrices according*  
 166 *to the adaption law given by equations (15) and (16).*

*Proof.* The observer error dynamics is given by:

$$\begin{aligned}\dot{\tilde{\sigma}} &= \tilde{\chi}(t) - K_1\Phi_1(\tilde{\sigma}) \\ \dot{\tilde{\chi}} &= -K_2\Phi_2(\tilde{\sigma}) - h(t)\end{aligned} \quad (17)$$

Now, let us rename the error variables  $\tilde{\sigma}, \tilde{\chi}$  as follows :

$$\begin{aligned}s_{1i} &= \tilde{\sigma}_i \\ s_{2i} &= \tilde{\chi}_i\end{aligned}$$

Then, Eq. (17) can be rewritten in a scalar form ( $i = \overline{1, 6}$ ) as:

$$\begin{aligned}\dot{s}_{1i} &= -k_{1i} \left[ \mu_{1i}|s_{1i}|^{\frac{1}{2}}\text{sgn}(s_{1i}) + \mu_{2i}s_{1i} \right] + s_{2i} \\ \dot{s}_{2i} &= -k_{2i} \left[ \frac{1}{2}\mu_{1i}^2\text{sgn}(s_{1i}) + \frac{3}{2}\mu_{1i}\mu_{2i}|s_{1i}|^{\frac{1}{2}}\text{sgn}(s_{1i}) + \mu_{2i}^2s_{1i} \right] + h_i(t)\end{aligned} \quad (18)$$

Without loss of generality, we can represent the system (18) with the following simplified notation:

$$\begin{aligned}\dot{s}_1 &= -k_1 \left[ \mu_1 |s_1|^{\frac{1}{2}} \text{sgn}(s_1) + \mu_2 s_1 \right] + s_2 \\ \dot{s}_2 &= -k_2 \left[ \frac{1}{2} \mu_1^2 \text{sgn}(s_1) + \frac{3}{2} \mu_1 \mu_2 |s_1|^{\frac{1}{2}} \text{sgn}(s_1) + \mu_2^2 s_1 \right] + h(t)\end{aligned}\quad (19)$$

Now, in order to prove the asymptotic stability of the closed-loop system (19), we propose the following Lyapunov function candidate:

$$V(s_1, s_2, k_1, k_2) = V_0(\cdot) + \frac{1}{2\varsigma_1} (k_1 - k_1^*)^2 + \frac{1}{2\varsigma_2} (k_2 - k_2^*)^2 \quad (20)$$

where  $\varsigma_1, \varsigma_2, k_1^*$ , and  $k_2^*$  are positive constants and  $V_0(\cdot)$  is given by:

$$V_0(s_1, s_2, k_1, k_2) = \xi^T P \xi \quad (21)$$

with:

$$\xi^T = [\phi_1(s_1), s_2] \quad (22)$$

and

$$P = P^T = \begin{bmatrix} \beta + 4\epsilon^2 & -2\epsilon \\ -2\epsilon & 1 \end{bmatrix} > 0 \quad (23)$$

Since  $\beta$  and  $\epsilon$  are defined as arbitrary positive constants,  $P$  is a positive definite matrix. Clearly, the quadratic form  $V_0(\cdot)$  satisfies:

$$\lambda_{\min}(P) \|\xi\|_2^2 \leq V_0(s, k) \leq \lambda_{\max}(P) \|\xi\|_2^2 \quad (24)$$

where  $\lambda_{\min}(P)$  and  $\lambda_{\max}(P)$  respectively are the smallest and greatest eigenvalue of  $P$ .  $\|\xi\|_2^2 = \mu_1^2 |s_1| + 2\mu_1 \mu_2 |s_1|^{\frac{3}{2}} + \mu_2^2 s_1^2 + s_2^2$  is the Euclidean norm of  $\xi$  and the next inequality is satisfied as well:

$$|\phi(s_1)| \leq \|\xi\|_2 \leq \frac{V^{\frac{1}{2}}(\xi)}{\lambda_{\min}^{\frac{1}{2}}(P)} \quad (25)$$

167 Finally, it is important to note that the proposed candidate Lyapunov func-  
168 tion  $V(s_1, s_2, k_1, k_2)$  is a continuous, positive definite and differentiable func-  
169 tion.

170 To compute the time derivative of the proposed Lyapunov function can-  
 171 didate (20), the time derivative of  $V_0(\cdot)$  is found first. Then, the total time  
 172 derivative of  $V(\cdot)$  is computed:

**Step 1.** Noting that  $\phi_2(s_1) = \phi_1'(s_1)\phi_1(s_1)$ , where  $\phi_1'(s_1) = \left(\mu_1 \frac{1}{2|s_1|^{1/2}} + \mu_2\right)$ , and introducing  $L = \frac{h(t)}{\phi_1'(s_1)}$ . Then, the time derivative of  $V_0(\cdot)$  is obtained as:

$$\dot{V}_0 = 2\xi^T P \dot{\xi} \quad (26)$$

$$= 2\xi^T P \begin{bmatrix} \phi_1' \left[ -k_1 \phi_1(s_1) + s_2 \right] \\ -k_2 \phi_2(s_1) + h(t) \end{bmatrix} \quad (27)$$

$$= 2\xi^T P \begin{bmatrix} \phi_1'(s_1) \left[ -k_1 \phi_1(s_1) + s_2 \right] \\ \phi_1'(s_1)\phi_1(s_1) \left[ -k_2 + L \right] \end{bmatrix} \quad (28)$$

$$= \phi_1'(s_1) 2\xi^T P \underbrace{\begin{bmatrix} -k_1 & s_2 \\ -(k_2 - L) & 0 \end{bmatrix}}_{A(t, \chi)} \xi \quad (29)$$

$$= \phi_1'(s_1) \xi^T (A^T(t, \chi)P + PA(t, \chi))\xi \quad (30)$$

$$= -\phi_1'(s_1) \xi^T Q(t, \chi)\xi \quad (31)$$

where

$$Q(t, \chi) = \begin{bmatrix} 2k_1(\beta + 4\epsilon^2) - 4\epsilon(k_2 - L) & \star \\ k_2 - L - 2\epsilon k_1 - \beta - 4\epsilon^2 & 2\epsilon \end{bmatrix} \quad (32)$$

173 and  $\star = k_2 - L - 2\epsilon k_1 - \beta - 4\epsilon^2$ .

Selecting the gain  $k_2 = 2\epsilon k_1 + \beta + 4\epsilon^2$ , we have:

$$Q - 2\epsilon I = \begin{bmatrix} 2k_1\beta - 4\epsilon(\beta + 4\epsilon^2 - L) - 2\epsilon & -L \\ -L & 2\epsilon \end{bmatrix} \quad (33)$$

The matrix  $Q$  will be positive definite with a minimal eigenvalue  $\lambda_{\min}(Q) \geq 2\epsilon$  if

$$k_1 > \delta_0 + \frac{\alpha_2^2}{4\epsilon\beta} + \frac{\epsilon \left[ 2(\beta + 4\epsilon^2 + L) + 1 \right]}{2\beta} \quad (34)$$

174 where  $\delta_0$  is a small positive constant.

Then, the time derivative of  $V_0(\cdot)$  can be rewritten as:

$$\dot{V}_0 = -\phi_1'(s_1)\xi^T Q(t, x)\xi \leq -2\epsilon\phi_1'(s_1)\xi^T \xi = -2\epsilon \left( \mu_1 \frac{1}{2|s_1|^{\frac{1}{2}}} + \mu_2 \right) \xi^T \xi \quad (35)$$

Finally, using Eq. (25), the time derivative of  $V_0(\cdot)$  is expressed as:

$$\dot{V}_0 \leq -\frac{\epsilon\lambda_{\min}^{\frac{1}{2}}(P)}{\lambda_{\max}(P)}\mu_1 V_0^{\frac{1}{2}}(s, k) - \frac{2\epsilon}{\lambda_{\max}(P)}\mu_2 V(s, k) \quad (36)$$

$$\leq -\gamma V_0^{\frac{1}{2}}(s, k) \quad (37)$$

175 with  $\gamma = \mu_1 \frac{\epsilon\lambda_{\min}^{\frac{1}{2}}(P)}{\lambda_{\max}(P)}$ .

**Step 2.** The time derivate of the Lyapunov function candidate (20) is obtained as follows:

$$\dot{V} = \dot{V}_0(\cdot) + \frac{1}{\varsigma_1}(k_1 - k_1^*)\dot{k}_1 + \frac{1}{\varsigma_2}(k_2 - k_2^*)\dot{k}_2 \quad (38)$$

$$\leq -\gamma V_0^{\frac{1}{2}}(s, k) + \frac{1}{\varsigma_1}(k_1 - k_1^*)\dot{k}_1 + \frac{1}{\varsigma_2}(k_2 - k_2^*)\dot{k}_2 \quad (39)$$

$$= -\gamma V_0^{\frac{1}{2}}(s, k) - \frac{\omega_1}{\sqrt{2\varsigma_1}}|k_1 - k_1^*| - \frac{\omega_2}{\sqrt{2\varsigma_2}}|k_2 - k_2^*| + \frac{1}{\varsigma_1}(k_1 - k_1^*)\dot{k}_1 + \quad (40)$$

$$+ \frac{1}{\varsigma_2}(k_2 - k_2^*)\dot{k}_2 + \frac{\omega_1}{\sqrt{2\varsigma_1}}|k_1 - k_1^*| + \frac{\omega_2}{\sqrt{2\varsigma_2}}|k_2 - k_2^*| \quad (41)$$

Using the inequality  $\sqrt{x^2 + y^2 + z^2} \leq |x| + |y| + |z|$ , the first three terms of  $\dot{V}$  can be synthesized as follows:

$$-\gamma V_0^{\frac{1}{2}}(s, k) - \frac{\omega_1}{\sqrt{2\varsigma_1}}|k_1 - k_1^*| - \frac{\omega_2}{\sqrt{2\varsigma_2}}|k_2 - k_2^*| \leq -\pi\sqrt{V(s, k_1, k_2)} \quad (42)$$

176 where  $\pi = \min(\gamma, \omega_1, \omega_2)$ .

Assuming that there exist positive constants  $k_1^*$  and  $k_2^*$  such that  $k_1 - k_1^* < 0$  and  $k_2 - k_2^* < 0$  are satisfied  $\forall t \geq 0$ . Then, the time derivative of  $V$  can be rewritten as:

$$\begin{aligned} \dot{V} &\leq -\pi\sqrt{V(s, k_1, k_2)} - |k_1 - k_1^*| \left( \frac{1}{\varsigma_1}\dot{k}_1 - \frac{\omega_1}{\sqrt{2\varsigma_1}} \right) - |k_2 - k_2^*| \left( \frac{1}{\varsigma_2}\dot{k}_2 - \frac{\omega_2}{\sqrt{2\varsigma_2}} \right) \\ &= -\pi\sqrt{V(s, k_1, k_2)} + \vartheta \end{aligned} \quad (43)$$

where:

$$\vartheta = -|k_1 - k_1^*| \left( \frac{1}{\varsigma_1} \dot{k}_1 - \frac{\omega_1}{\sqrt{2\varsigma_1}} \right) - |k_2 - k_2^*| \left( \frac{1}{\varsigma_2} \dot{k}_2 - \frac{\omega_2}{\sqrt{2\varsigma_2}} \right) \quad (44)$$

In order to preserve the finite time convergence, it is necessary to ensure the condition  $\vartheta = 0$ , which will be achieved through the following adaption laws:

$$\dot{k}_1 = \omega_1 \sqrt{\frac{\varsigma_1}{2}} \quad (45)$$

$$\dot{k}_2 = \omega_2 \sqrt{\frac{\varsigma_2}{2}} \quad (46)$$

177 In brief, the adaptive gains  $k_1$  and  $k_2$  will be increased based on the dy-  
 178 namic and algebraic equations stated in (15)-(16), until the condition (34)  
 179 is reached. Then, the matrix  $Q$  will be positive definite and the finite time  
 180 convergence will be assured according to (43). The previous result guaran-  
 181 tees the finite time convergence of  $\tilde{\sigma}$  and  $\tilde{\chi}$  to zero, and when this happens,  
 182 the adaptive gains  $k_1$  and  $k_2$  will stop growing by making  $\dot{k}_1 = 0$ .  $\square$

183 **Remark 2.** *In real applications, an 'ideal' sliding mode cannot be established*  
 184 *[30]. Then, it is crucial to introduce the concept of the 'real' sliding mode.*

185 **Definition 1.** *Given the sliding variable  $\tilde{\sigma}(t)$ , the 'real sliding surface'*  
 186 *associated with (9) is defined as in the sense of [31].*

*In this context, the definition of 'real' sliding mode means that the con-  
 dition  $\tilde{\sigma}(t) = 0$  is never satisfied. In fact, the variable  $\tilde{\sigma}(t)$  is related to the  
 system state  $\eta$  as stated by Eq. (11). Then, the measurement of  $\eta$  is always  
 corrupted by noise, which makes impossible the satisfaction of the condition  
 $\tilde{\sigma}(t) = 0$ . Therefore, the gains  $k_1(t)$  and  $k_2(t)$  given by Eqs. (15) and (16)  
 will increase drastically. To overcome this drawback, the definition of the real  
 sliding surface is employed, and the adaptive gains (15)-(16) are modified as  
 follows:*

$$\dot{k}_{1i}(t) = \begin{cases} 0 & \text{if } |\tilde{\sigma}| < \delta_i \\ \mu_{1i} \sqrt{\frac{\varsigma_{1i}}{2}} & \text{otherwise} \end{cases} \quad (47)$$

$$k_{2i}(t) = 2\epsilon_i k_{1i}(t) + \beta_i + 4\epsilon_i^2 \quad (48)$$

187 where  $\delta_i$  is a small positive parameter.

188 **Remark 3.** *The selection of the parameter  $\delta_i$  was chosen by trial and error*  
189 *approach. However, there is a trade-off between the parameter value selec-*  
190 *tion and the chattering effect in the robot's actuators caused by the gain*  
191 *overestimation. This means that if  $\delta_i$  is selected close to zero, the feedback*  
192 *controller's gains will grow up, and if the the parameter is selected too high,*  
193 *the convergence time of the robot to the reference trajectory will increase as*  
194 *well.*

#### 195 4. Enhanced Controller design

196 In this section, a brief description of the enhanced backstepping and non-  
197 linear PD controllers is provided. First, The adaptive disturbance observer is  
198 introduced into the controllers in order to counteract the effects of the exter-  
199 nal disturbances and parameter uncertainties. Then, Lyapunov's functions  
200 are used to prove the stability of the controller/observer scheme.

##### 201 4.1. Adaptive Backstepping controller

202 The design of a Backstepping controller for trajectory tracking in-depth  
203 and yaw dynamics was proposed in work [14]. In this study, the authors  
204 demonstrated the effectiveness of the proposed controller through real-time  
205 experiments. However, from the depth tracking experimental results, one can  
206 notice that there is a tracking offset between the controller signal and the  
207 trajectory reference. This deficiency can be due to a bad tuning or that the  
208 force of the disturbance is excessive and, therefore, exceeds the capabilities  
209 of the proposed control. In order to overcome this drawback, in this section,  
210 the disturbance estimation made by the AGSTA-ESO is inserted into the  
211 algorithm shown in [14]. As a result of the proposed scheme, the Adaptive  
212 Backstepping control (ABS) is described in the following theorem:

213 **Theorem 2.** *Consider the system (7) transformed into (9). Let  $e_1(t) = \zeta_1 -$*   
214  *$\zeta_1^d$  and  $e_2(t) = [e_2^x(t), e_2^y(t), \dots, e_2^\psi(t)]^T = \dot{e}_1(t) + \Gamma e_1(t)$  be the tracking errors*  
215 *and the gain diagonal and positive definite matrices  $\Gamma = \text{diag}(\gamma_1, \gamma_2, \dots, \gamma_6)$*   
216 *and  $\Upsilon = \text{diag}(v_1, v_2, \dots, v_6)$ . If Assumptions 1 and 2 are satisfied and*  
217 *proposing the following adaptive backstepping controller:*

$$\tau_\eta = G(\zeta)^{-1} \left[ \ddot{\eta}^d - e_1 - \overline{F}(\zeta) + \Gamma (\Gamma e_1 - e_2) - \Upsilon e_2 - \hat{d} - \hat{K} \text{Sign}(e_2) \right] \quad (49)$$

where  $\hat{d}(t)$  is the estimation of the disturbance made by the AGSTA-ESO (14),  $Sign(e_2(t)) = [sgn(e_2^x(t)), sgn(e_2^y(t)), \dots, sgn(e_2^\psi(t))]^T$ , and  $\hat{K}$  is a constant gain selected by the following adaption law:

$$\dot{\hat{K}} = \lambda_1 \|e_2(t)\| \quad (50)$$

218 with  $\lambda_1$  is a positive constant. Then, the tracking errors  $e_1(t)$  and  $e_2(t)$   
219 converge to zero asymptotically.

*Proof. Step 1.* Let us consider the following Lyapunov function candidate:

$$V_1(e_1) = \frac{1}{2} e_1^T e_1 \quad (51)$$

The time derivative of  $V$  along the trajectories of the system (9) is given by:

$$\dot{V}(e_1) = e_1^T \dot{e}_1 = e_1^T (\dot{\zeta}_1 - \dot{\zeta}_1^d) = e_1^T (\zeta_2 - \dot{\zeta}_1^d) \quad (52)$$

Selecting  $\zeta_2$  as the virtual control,  $\zeta_2^v$ , as follows:

$$\zeta_2^v = \dot{\zeta}_1^d - \Gamma e_1 \quad (53)$$

yields to:

$$\dot{V}_1(e_1) = -e_1^T \Gamma e_1 \quad (54)$$

220 Moreover, the stabilization of  $\dot{e}_1(t)$  is achieved by choosing  $\Gamma > 0$ .

**Step 2.** Introducing the following error  $e_2 = \zeta_2 - \zeta_2^v$ , and computing its time derivative with (53), yields to the following dynamic error system:

$$\dot{e}_1 = e_2 - \Gamma e_1 \quad (55)$$

$$\dot{e}_2 = \bar{F}(\zeta) + G(\zeta)u + d(t) - \ddot{\zeta}_1^d + \Gamma \dot{e}_1 \quad (56)$$

Proposing the Lyapunov function candidate as:

$$V_2(e_1, e_2) = \frac{1}{2} e_1^T e_1 + \frac{1}{2} e_2^T e_2 + \frac{1}{2\lambda_1} \tilde{K}^2 \quad (57)$$

221 where the parameter estimation error is defined as  $\tilde{K} = \hat{K} - K$ .

The time derivative of  $V_2$  along the trajectories over the system (55) is obtained as follows:

$$\dot{V}_2 = e_1^T \dot{e}_1 + e_2^T \dot{e}_2 + \frac{1}{\lambda_1} \tilde{K} \dot{K} \quad (58)$$

$$= e_1^T [e_1 - \Gamma e_1] + e_2^T [\bar{F}(\zeta) + G(\zeta)\tau_\eta + d(t) - \ddot{\zeta}_1^d + \Gamma \dot{e}_1] + \frac{1}{\lambda_1} \tilde{K} \dot{K} \quad (59)$$

$$= -e_1^T \Gamma e_1 + e_2^T [e_1 + \bar{F}(\zeta) + G(\zeta)\tau_\eta + d(t) - \ddot{\zeta}_1^d + \Gamma \dot{e}_1] + \frac{1}{\lambda_1} \tilde{K} \dot{K} \quad (60)$$

Injecting the control law (49) into the time derivative of  $V_2$ , and assuming that the AGSTA-ESO estimates the external disturbance in finite time and fulfills the following constraint  $\|d(t) - \hat{d}(t)\| \leq K$  [32], leads to

$$\dot{V}_2 = -e_1^T \Gamma e_1 - e_2^T \Upsilon e_2 + e_2^T [d(t) - \hat{d}(t) - \hat{K} Sgn(e_2)] + \frac{1}{\lambda_1} \tilde{K} \dot{K} \quad (61)$$

$$\leq -\lambda_{min}(\Gamma) \|e_1\|_2^2 - \lambda_{min}(\Upsilon) \|e_2\|_2^2 + \|e_2\|_2 K - \|e_2\|_2 \hat{K} + \tilde{K} \|e_2\|_2 \quad (62)$$

$$= -\lambda_{min}(\Gamma) \|e_1\|_2^2 - \lambda_{min}(\Upsilon) \|e_2\|_2^2 \quad (63)$$

222 Finally, the asymptotic stabilization of the closed loop system is guaranteed  
223 selecting  $\Gamma > 0$  and  $\Upsilon > 0$ .  $\square$

**Remark 4.** For comparison purpose, the Backstepping control law developed in work [14] is given by the following:

$$\tau_\eta = G(\zeta)^{-1} [\ddot{\eta}^d - e_1(t) - \bar{F}(\zeta) + \Gamma (\Gamma e_1(t) - e_2(t)) - \Upsilon e_2(t)] \quad (64)$$

#### 224 4.2. Adaptive Nonlinear PD control

The NLPD is a robust controller proposed in work [18]. The authors have proven the robustness of the NLPD to parametric uncertainties. However, based on the experimental results, due to the extra damping added to the vehicle, the performance of the depth tracking shows a constant error during the steady-state behavior. In order to overcome this drawback, it was shown in Guerrero et al. [29] that, the addition of a finite-time disturbance estimator, GSTA-ESO, to the nominal NLPD improves significantly its effectiveness towards external and parametric disturbances. In this vein, one step ahead might be the introduction of adaptation laws allowing to update the observer's gains depending on the disturbance evolution. The advantage is that the controller will be able of rejecting bounded time-varying disturbances even if the upper bound of the perturbation is not known. Following

this line of thinking, the disturbance estimation made by the AGSTA-ESO will be introduced into the NLPD.

For notation consistency, let us now write the UAV's dynamic system (9) in terms of the variables  $\zeta_1 = \eta$  and  $\zeta_2 = \dot{\eta}$ , namely,

$$\hat{M}_\zeta(\zeta)\dot{\zeta}_2 + \hat{C}_\zeta(\nu, \zeta_1)\dot{\zeta}_1 + \hat{D}_\zeta(\nu, \zeta_1)\zeta_1 + \hat{g}_\zeta(\zeta_1) = \tau_\zeta + \bar{d}(t) \quad (65)$$

225

226 The following Theorem gives the main result of this Section:

**Theorem 3.** *Let the vehicle's mathematical model with external disturbances be defined by Eq. (7), which can be rewritten into the model (65). Introducing the disturbance estimation  $\hat{d}(t)$  given by equations (14) into the following adaptive nonlinear PD (ANLPD) controller*

$$\begin{aligned} \tau_\zeta = & \hat{M}_\zeta \dot{\zeta}_2^d(t) + \hat{C}_\zeta(\nu, \zeta) \dot{\zeta}_1^d(t) + \hat{D}_\zeta(\nu, \eta) \zeta_1^d(t) + \hat{g}_\zeta(\zeta) - \\ & - K_p(\cdot)e - K_d(\cdot)\dot{e} - \hat{M}_\eta(\eta)\hat{d} - \hat{K} \text{Sign}(\dot{e}) \end{aligned} \quad (66)$$

where  $\zeta_2^d(t) = \dot{\zeta}_1^d(t)$ ,  $e(t) = [e_1(t), e_2(t), \dots, e_6(t)]^T = \zeta_1(t) - \zeta_1^d(t)$  is the error signal,  $\dot{e}(t) = [\dot{e}_1(t), \dot{e}_2(t), \dots, \dot{e}_6(t)]^T = \dot{\zeta}_1(t) - \dot{\zeta}_1^d(t)$  its time derivative, and the desired trajectory is defined as  $\zeta_1^d(t) = [x_d(t), y_d(t), z_d(t), \phi_d(t), \theta_d(t), \psi_d(t)]^T$ . The vector  $\text{Sign}(\dot{e}) = [\text{sgn}(\dot{e}_1(t)), \text{sgn}(\dot{e}_2(t)), \dots, \text{sgn}(\dot{e}_6(t))]$ ,  $d(t) = \hat{M}(\eta)^{-1}\bar{d}(t)$ , and  $\hat{K}$  is a constant gain selected by the following adaption law:

$$\dot{\hat{K}} = \lambda_2 \|e_2(t)\| \quad (67)$$

where  $\lambda_2$  is a positive constant. The gain matrices  $K_p(\cdot)$  and  $K_d(\cdot)$  have the following structure:

$$K_p(\cdot) = \begin{bmatrix} k_{p1}(\cdot) & 0 & \cdots & 0 \\ 0 & k_{p2}(\cdot) & \cdots & 0 \\ \vdots & \vdots & \ddots & \vdots \\ 0 & 0 & \cdots & k_{pn}(\cdot) \end{bmatrix} > 0 \quad (68)$$

$$K_d(\cdot) = \begin{bmatrix} k_{d1}(\cdot) & 0 & \cdots & 0 \\ 0 & k_{d2}(\cdot) & \cdots & 0 \\ \vdots & \vdots & \ddots & \vdots \\ 0 & 0 & \cdots & k_{dn}(\cdot) \end{bmatrix} > 0 \quad (69)$$

and asymptotically stabilize the system (7) if the underwater vehicle is moving at low speed, and if  $k_{pj}(\cdot)$  and  $k_{dj}(\cdot)$  are defined as:

$$k_{pj}(\cdot) = \begin{cases} b_{pj}|e_j(t)|^{(\mu_{pj}-1)} & \text{if } |e_j(t)| > d_{pj} \\ b_{pj}d_{pj}^{(\mu_{pj}-1)} & \text{if } |e_j(t)| \leq d_{pj} \end{cases} \quad (70)$$

$$k_{dj}(\cdot) = \begin{cases} b_{dj}|\dot{e}_j(t)|^{(\mu_{dj}-1)} & \text{if } |\dot{e}_j(t)| > d_{dj} \\ b_{dj}d_{dj}^{(\mu_{dj}-1)} & \text{if } |\dot{e}_j(t)| \leq d_{dj} \end{cases} \quad (71)$$

$$\forall \mu_{pj}, \mu_{dj} \in [0, 1].$$

227 with the positive constants  $b_{pj}$ ,  $b_{dj}$ ,  $d_{pj}$ , and  $d_{dj}$ .

*Proof.* Injecting the control law (66) into the mathematical model of the underwater vehicle, (9), the closed-loop error system is given by:

$$\frac{d}{dt} \begin{bmatrix} e \\ \dot{e} \end{bmatrix} = \begin{bmatrix} \dot{e} \\ -\hat{M}_\zeta(\eta)^{-1} \left[ [\hat{C}_\zeta + \hat{D}_\zeta + K_d(\cdot)]\dot{e} + K_p(\cdot)e + \hat{K}Sgn(\dot{e}) \right] - \hat{d}(t) + d(t) \end{bmatrix} \quad (72)$$

Let us consider the following Lyapunov candidate function as:

$$V(e, \dot{e}) = \frac{1}{2} \dot{e}^T \hat{M}_\zeta(\zeta) \dot{e} + \int_0^e \varrho^T K_p(\varrho) d\varrho + \frac{1}{2\lambda_2} \tilde{K}^2 \quad (73)$$

where

$$\int_0^e \varrho^T K_p(\varrho) d\varrho = \int_0^{e_1} \varrho^T K_p(\varrho) d\varrho + \int_0^{e_2} \varrho^T K_p(\varrho) d\varrho + \dots + \int_0^{e_6} \varrho^T K_p(\varrho) d\varrho \quad (74)$$

228 and  $\kappa$  is a positive constant.

This function is positive definite and radially unbounded (see [18] for a deeper description). Then, the time derivative of the Lyapunov candidate function is computed as:

$$\dot{V}(e, \dot{e}) = \dot{e}^T \hat{M}_\zeta(\zeta) \ddot{e} + \frac{1}{2} \dot{e}^T \dot{\hat{M}}_\zeta(\zeta) \dot{e} + e^T K_p(\cdot) \dot{e} + \frac{1}{\lambda_2} \tilde{K} \dot{\tilde{K}} \quad (75)$$

Considering that the GSTA-ESO converges to the disturbance dynamics in finite time, it is reasonable to assume that  $\|d(t) - \hat{d}(t)\| \leq K$ , with the unknown constant  $K > 0$ . The constant  $K$  was obtained through the adaption

law (67). Then, substituting the error dynamics (72) into the time derivative of  $V(\cdot)$  and considering the Assumption 2 and equation (67), yields to:

$$\dot{V}(e, \dot{e}) = -\dot{e}^T \left[ \hat{D}_\zeta(\nu, \zeta) + K_d(\cdot) \right] \dot{e} + \dot{e}^T [d(t) - \hat{d}(t)] - \hat{K} \dot{e}^T \text{Sign}(\dot{e}) + \frac{1}{\lambda_2} \tilde{K} \dot{K} \quad (76)$$

$$= -\dot{e}^T \left[ \hat{D}_\zeta(\nu, \zeta) + K_d(\cdot) \right] \dot{e} + \dot{e}^T [d(t) - \hat{d}(t)] - \hat{K} \sum_{i=0}^6 |\dot{e}_i| + \frac{1}{\lambda_2} \tilde{K} \dot{K} \quad (77)$$

$$\leq -\lambda_{\min}(\hat{D}_\zeta(\nu, \zeta) + K_d(\cdot)) \|\dot{e}\|^2 + K \|\dot{e}\| - \hat{K} \|\dot{e}\| + \tilde{K} \|\dot{e}\| \quad (78)$$

$$\leq -\lambda_{\min}(\hat{D}_\zeta(\nu, \zeta) + K_d(\cdot)) \|\dot{e}\|^2 \quad (79)$$

229 Finally, because the gain matrix is  $K_d(\cdot) > 0$  by design and the damping  
 230 matrix fulfills  $\hat{D}_\zeta(\nu, \zeta) > 0$  [4], the function  $\dot{V}(\cdot)$  is negative semi-definite.  
 231 Finally, applying the Krasovskii-Lasalle's theorem we can conclude that the  
 232 equilibrium point is asymptotically stable [18].  $\square$

**Remark 5.** *In the experimental part of this work, the performance of the developed controller law given by equation (66) is compared to the NLPD control proposed in [18], namely:*

$$\tau_\zeta = \hat{M}_\zeta \dot{\zeta}_2^d(t) + \hat{C}_\zeta(\nu, \zeta) \dot{\zeta}_1^d(t) + \hat{D}_\zeta(\nu, \eta) \zeta_1^d(t) + \hat{g}_\zeta(\zeta) - K_p(\cdot)e - K_d(\cdot)\dot{e} \quad (80)$$

233 **Remark 6.** *It is worth to notice that in this manuscript is different from*  
 234 *the work presented in [19]. On one hand, in study [19], a nonlinear PID was*  
 235 *proposed while in this work, we propose the improvement of the nonlinear PD*  
 236 *proposed by [18]. On the other hand, in this manuscript, we use sliding mode*  
 237 *theory to improve a PD controller while in work [19] is an extension of the*  
 238 *saturated based-control.*

## 239 5. Experimental Results

240 *Leonard* is a tethered underwater vehicle entirely designed and built at  
 241 LIRMM (University of Montpellier / CNRS, France). The vehicle's size is 75  
 242 cm long, 55 cm width, and 45 cm height and weighs 28 kg. The propulsion  
 243 system of this vehicle consists of six independent thrusters to obtain a fully  
 244 actuated system.

245 The information from the sensors of the underwater vehicle (depth, IMU)  
246 is sent, through a tether, to a computer located at the surface. Then, the ma-  
247 chine computes the control laws and sends the control input to each thruster  
248 of *Leonard*. The computer machine is a laptop with Intel Core i7-3520M 2.9  
249 GHz CPU, 8GB of RAM, it runs under Windows 7 operating system, and  
250 the control software is developed using Visual C++ 2010. More details about  
251 the *Leonard* Underwater Vehicle can be found in [22].

252 The real-time experiments have been carried out in the  $4 \times 4 \times 1.2$  m pool of  
253 the LIRMM. Even though the proposed control laws were given by equations  
254 (49), (64), (66) and (80) is designed for the whole system (six degrees of  
255 freedom), the experiments conducted in this study concern only depth and  
256 yaw trajectory tracking. The primary goal of the proposed controllers is to  
257 track the desired reference trajectory robustly in depth and yaw even in the  
258 presence of parameter uncertainties and external disturbances. The whole  
259 set of real-time experiments is available at:

260 <https://www.youtube.com/watch?v=aBOvvlvYNQE>

261 <https://www.youtube.com/watch?v=oXPqSLvXobk>

### 262 5.1. Proposed Scenarios

263 In order to show the improvement of adding the adaptive finite time  
264 disturbance estimator to the BS and NLPD controllers, we propose three  
265 main scenarios:

266 (i) Scenario 1: Nominal case.

267 In this scenario, the robot follows a predefined desired trajectory in  
268 depth and yaw in the absence of external disturbances. During this  
269 test, the controller's gains are adjusted to obtain the best tracking.  
270 These gains remain unchanged during the rest of the experiments.

271 (ii) Scenario 2: Robustness towards parametric uncertainties

272 In this test, the buoyancy and damping of the vehicle are increased to  
273 test the robustness of the proposed methodology towards parametric  
274 uncertainties, see Figure 2.

275 (iii) Scenario 3: External disturbances rejection.

276 In this test, the vehicle has the task of loading an object and when  
277 reaching a certain depth, dropping that object. Moreover, during this  
278 test, it is possible to see a sudden change in the vehicle's weight and  
279 how it affects the controller performance, see Figure 3.

280 *5.2. Feedback controller gains tuning*

281 It is worth to notice that the selection of the tuning gains of the BS and  
 282 NLPD controllers were found following the procedure proposed in [14] and  
 283 [18], respectively.

284 For the tuning of the proposed adaptive observer gains given by Eq. (15) ,  
 285 we found the gains by heuristic approach, the steps are shown below:

286

- 287 1. We set the value of  $\varsigma_{1i} = 1$  and  $\mu_{1i} = 0.1$ . Note that  $\mu_{1i}$  is the main  
 288 parameter to modify the value of  $k_{1i}$ .
- 289 2. The gain  $k_{2i}$  is related to the estimation of the disturbance. In this  
 290 vein, we set  $\epsilon_i$  to a small value ( $\epsilon_i = 0.1$ ) in order to limit the growth  
 291 of  $k_{2i}$ . Also, we use  $\beta_i$  to modify the value of  $k_{2i}$ .
- 292 3. It is worth to note that the ideal sliding surface does not exist, then,  $\tilde{\sigma} =$   
 293  $0$  is never reached and  $\delta_i$  is a nonzero constant. Initially, the value of  $\delta_i$   
 294 is set to a small value. This parameter needs to be adjusted depending  
 295 of the behavior of the robot during experiments. For instance, if the  
 296 gains increase fast, this value needs to be increased as well.
- 297 4. Finally, the parameter  $\Lambda_i$  is used to modify the convergence rate of  
 298 the robot to the reference trajectory. As explained above, this value  
 299 can be set to  $\Lambda = 1$  and it will be increased to improve the controller  
 300 performance.

301 **Remark 7.** *The adaption law of  $\hat{K}$  is obtained through the integration of*  
 302 *Equations (50) or (67). One can notice that the adaption depends on the*  
 303 *norm of the time derivative of the tracking error and the gains  $\lambda_1$  or  $\lambda_2$ .*  
 304 *Then, in order to minimize the chattering effect due to the signum function*  
 305 *into the control law, it is suggested to keep the gains  $\lambda_1$  and  $\lambda_2$  as small as*  
 306 *possible. In the real-time experiments, the gains were considered as  $\lambda_1 \rightarrow 0$*   
 307 *and  $\lambda_2 \rightarrow 0$ , which yields to  $\hat{K} \rightarrow 0$ . The Tables 1-4 show the gains for the*  
 308 *proposed observer and controllers.*

309 **Remark 8.** *Note that at first sight, the proposed controller have several gains*  
 310 *to tune, however, most of the parameters can be set to zero or to a small value.*  
 311 *Based on the theoretical results of the main theorem, if the gains are selected*  
 312 *as in Eq. (15), the robot will converge to the reference trajectory.*

Depth	$\gamma_3 = 3.0$	$v_3 = 1.9$
Yaw	$\gamma_6 = 16.34$	$v_6 = 36.65$

Table 1: BS control gains used in real-time experiments

Depth	$\mu_3 = 0.1$	$\varsigma_3 = 1.0$	$\Lambda_3 = 2.0$
	$\epsilon_3 = 0.1$	$\beta_3 = 0.33$	$\delta_3 = 0.01$
Yaw	$\mu_6 = 0.1$	$\varsigma_6 = 1.0$	$\Lambda_6 = 3.5$
	$\epsilon_6 = 0.1$	$\beta_6 = 0.01$	$\delta_6 = 0.2$

Table 2: Adaptive disturbance observer gains for the BS scheme

### 313 5.3. Tracking Performance Indexes

In order to evaluate the tracking performance of the proposed controllers, let us compute the Root Mean Square Error (RMSE) as follows:

$$RMS(\cdot(t)) = \sqrt{\frac{1}{T_f} \int_0^{T_f} |\cdot(t)|^2 dt} \quad (81)$$

In addition, the integral of control inputs (the applied force and torque) are computed to estimated the energy consumption used in each case, that is:

$$INT = \int_{t_1}^{t_2} |\tau(t)| dt \quad (82)$$

314 where  $t_1 = 3 s$  and  $t_2 = 50 s$ .

315 In the rest of the paper, the RMSE for yaw and depth are defined as  
 316  $RMSE_\psi$ ,  $RMSE_z$ , respectively. The expressions  $INT_\psi$  and  $INT_z$  are the  
 317 integral control input of yaw and depth, respectively.

318 The estimated values for the integral are listed in Tables 7-8.

### 319 5.4. Scenario 1: Nominal Case

320 In this test, the submarine *Leonard* follows a predefined trajectory in  
 321 depth and heading at the same time. For the depth test, the robot goes from  
 322 the surface to a depth of 30 cm. At this point, the vehicle remains stable  
 323 for 20 seconds, and then, it goes to 20 cm, where it remains until the end  
 324 of the test. For the heading task, the vehicle turns from its initial position  
 325 to 60 degrees, where it remains stable for 20 seconds. Then, the submarine

Depth	$b_{p3} = 20$	$d_{p3} = 0.05$	$\mu_{p3} = 0.1$
	$b_{p3} = 13$	$d_{p3} = 0.25$	$\mu_{p3} = 0.2$
Yaw	$b_{p3} = 4.5$	$d_{p3} = 0.015$	$\mu_{p3} = 0.2$
	$b_{p3} = 0.2$	$d_{p3} = 0.15$	$\mu_{p3} = 0.2$

Table 3: NLPD control gains used in real-time experiments

Depth	$\mu_3 = 0.1$	$\varsigma_3 = 1.0$	$\Lambda_3 = 2.0$
	$\epsilon_3 = 0.1$	$\beta_3 = 0.33$	$\delta_3 = 0.01$
Yaw	$\mu_6 = 0.1$	$\varsigma_6 = 1.0$	$\Lambda_6 = 2.0$
	$\epsilon_6 = 0.1$	$\beta_6 = 0.01$	$\delta_6 = 0.2$

Table 4: Adaptive disturbance observer gains for the NLPD scheme

326 turns to  $-60$  degrees in only 6 seconds, where the vehicle stays until the  
327 end of the trial. The top of Fig. 4 shows the trajectory tracking in depth  
328 and yaw for the nominal case. From the Fig. 4, one can notice that all  
329 the controllers have a good tracking performance, and this can be confirmed  
330 through the plot of the tracking errors, which is shown in the middle of the  
331 Fig. 4 and is numerically expressed for the RMSE measurement in Tables 5  
332 and 6. In fact, from the RMSE indicator is easy to observe the improvement  
333 when the adaptive observer is considered. Then, at the bottom of Fig. 4,  
334 the evolution of the control inputs is shown. Again, the behavior of all the  
335 proposed controllers remains similar.

336 The top of figures 6 and 8 show the evolution of the adaptive gains of  
337 the proposed disturbance observer. From these figures, we can observe that  
338 when the vehicle moves from the steady position to another point, the gains  
339 are automatically adjusted in order to minimize the tracking error.

340 In the top of figs. 9-10, the estimation made by the disturbance observer is  
341 shown. The estimation of the disturbance using the Backstepping controller  
342 is displayed in the upper part of Fig. 9, while the estimation employing  
343 the NLPD is shown at the top of Fig. 10. It is worth to note that both  
344 estimations provided by the observers are not precisely the same, this is  
345 reasonable because the controllers are different and do not have the same  
346 gains. Nevertheless, the shape of the estimated disturbance is similar for  
347 both cases.

Finally, to compute the energy consumption of each controller and to

establish a fair comparison, the nominal controller is compared against its improved version. For example, for the Backstepping controller case:

$$INT_z = \frac{INT_z(ABS)}{INT_z(BS)} = 1.02; \quad INT_\psi = \frac{INT_\psi(BS)}{INT_\psi(ABS)} = 1.18$$

This result means that the energy consumption for the trajectory tracking in depth is almost similar for both controllers. While the energy consumption for the tracking in heading for the nominal BS is 1.18 time higher than the energy consumption using the ABS. The following ratios gives the integral of control input indicator for the NLPD controller:

$$INT_z = \frac{INT_z(NLPD)}{INT_z(ANLPD)} = 1.02; \quad INT_\psi = \frac{INT_\psi(ANLPD)}{INT_\psi(NLPD)} = 1.16$$

348 The energy consumption for the tracking test in depth is similar for both con-  
 349 trollers. For the trajectory tracking in yaw, the consumption of the ANLPD  
 350 controller is 1.16 time higher than the energy consumption using the nominal  
 351 design.

### 352 5.5. Scenario 2: Robustness to parametric uncertainties

353 In this scenario, to demonstrate the robustness of the proposed adaptive  
 354 disturbance observer, the physical parameters of *Leonard* have been modified.  
 355 Firstly, two floaters have been attached to both sides of the submarine to  
 356 increase the buoyancy of the vehicle by +100%. Secondly, to increase the  
 357 rotational damping along z by approximately 90%, a large rigid sheet of  
 358 plastic that has a dimension of 45 × 10 cm has been attached on one side of  
 359 the submarine (see Fig. 2).

In the top of Fig. 5, one can observe the behavior of the proposed con-  
 trollers. From the Figure, it is possible to note that the nominal design of  
 the BS and NLPD shows an offset between the trajectory of the submarine  
 and the reference signal. The results shown in this work coincide with the  
 ones presented in [14] and [18]. In contrast with these previous results, the  
 introduction of the adaptive observer allows improving the performance of  
 the nominal control design by suppressing the signal offset. The improved  
 controllers are capable of following the reference trajectory despite the un-  
 certainties in the parameters. The plot of the tracking errors is shown in  
 the middle of Fig. 5 and the numerical expression of the errors are shown in  
 Tables 5 and 6. The evolution of the input signals is displayed at the bottom

of Fig. 5. As expected, at the beginning of the test, the improved version of the controllers demands more energy than the nominal designs, but once the reference is reached, the behaviors are similar for both schemes. The values of the integral of the control inputs for the tracking test using the BS and ABS control shows that the energy consumption is similar for both cases, and the following ratios also illustrate this:

$$INT_z = \frac{INT_z(ABS)}{INT_z(BS)} = 1.01; INT_\psi = \frac{INT_\psi(ABS)}{INT_\psi(BS)} = 1.0$$

For the case of the depth and yaw tracking using the NLPD and ANLPD, the ratios are given by

$$INT_z = \frac{INT_z(NLPD)}{INT_z(ANLPD)} = 1.04; INT_\psi = \frac{INT_\psi(ANLPD)}{INT_\psi(NLPD)} = 1.02$$

360 This means that the energy consumption of the NLPD control is only 1.04  
 361 times higher than the consumption of the ANLPD. Moreover, the energy  
 362 consumption for the heading tracking is also very similar for both method-  
 363 ologies.

364 The adaptive gains of the proposed observer for the ABS and ANLPD  
 365 controllers are shown in the middle of the Figures 6 and 8, respectively. The  
 366 estimated disturbance for the ABS is displayed at the middle of the Fig. 10,  
 367 while the estimation made by the ANLPD is shown at the middle of the Fig.  
 368 10. Again, the estimated disturbance shape is similar for both methods.

### 369 5.6. Scenario 3: Rejection of external disturbances

370 This test is inspired by a more realistic situation where the submarine  
 371 is equipped with a robotic manipulator. The main objective is to transport  
 372 an object from a certain depth to another where the submarine will release  
 373 the load. In this context, to simulate an object, we tie a metallic 1 kg block  
 374 to *Leonard* with a 20 cm-long line. In this test, the maximal depth has  
 375 been set to 40 cm. As the maximum depth of the basin is 50 cm, the robot  
 376 will be suddenly disturbed when it will reach 30 cm, because the metallic  
 377 block will touch the floor, thus suddenly canceling its weight's effect. The  
 378 disturbance will be acting on the robot until it starts to move up and reaches  
 379 30 cm. Then, the action of the extra weight will influence the trajectory of  
 380 the submarine again (see Fig. 3). This action simulates both the sudden  
 381 release and recovery of a load by the robot.

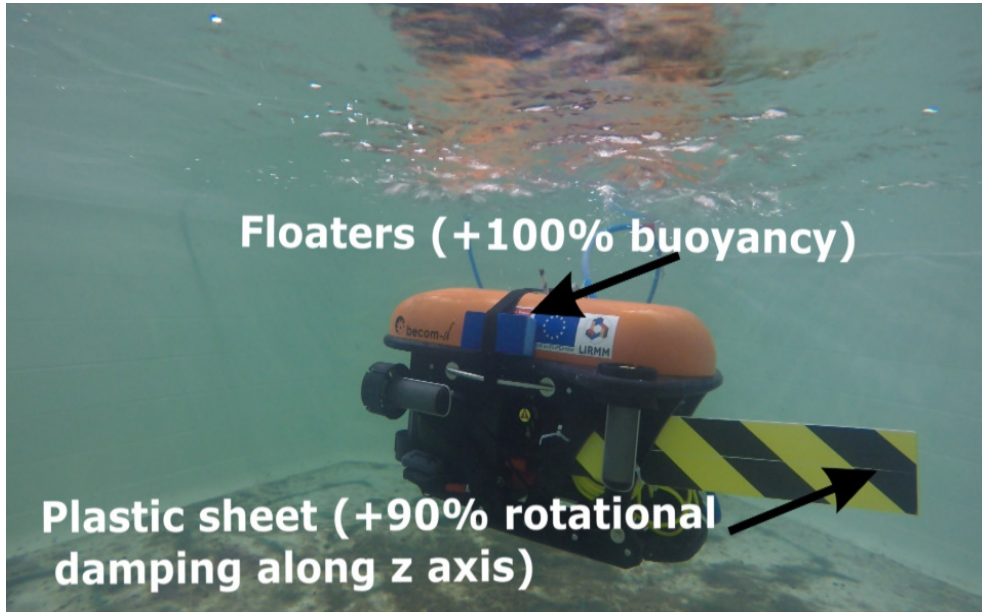


Figure 2: Modification of system parameters, increasing the buoyancy force and damping along z axis.

The performance of the proposed controllers is shown at the top of Fig. 7. From this figure, it can be noticed that although the behavior of the BS and the ABS is similar at the beginning of the test, the BS fails to track the reference signal efficiently when the robot tries to reach the 20 centimeters in depth. Moreover, the BS control has a 10 cm offset in the steady-state behavior. In contrast, the ABS takes some time to tune its gains itself, but once is achieved, the robot is able to follow the trajectory efficiently despite the weight of the load. In the same way, the NLPD fails to follow the reference. Indeed, this controller has the worst performance compared to all the others methodologies. Again, the introduction of the observer improves the behavior of the NLPD as can be seen in the top of Fig. 7. Concerning the trajectory tracking in yaw, the whole set of controllers show a good performance. The plot of the errors for both tracking tasks is displayed in the middle of Fig. 7, and its numerical representation is shown in Tables 5 and 6. At the bottom of Fig. 7, the evolution of the control inputs is displayed. While the performance of the BS and the ABS controllers are very similar, the ANLPD shows an aggressive behavior compared to the NLPD. Regarding energy consumption, using the BS requires 1.03 time more energy

than using the ABS for both tracking tests, as illustrated by the ratio below:

$$INT_z = \frac{INT_z(BS)}{INT_z(ABS)} = 1.03; \quad INT_\psi = \frac{INT_\psi(BS)}{INT_\psi(ABS)} = 1.03$$

The energy consumption using the ANLPD is 1.12 time the energy consumption using the NLPD for the depth tracking test. For the heading tracking task, the energy consumption employing the ANLPD is 1.09 times the energy consumption using the NLPD. The ratios are computed as:

$$INT_z = \frac{INT_z(ANLPD)}{INT_z(NLPD)} = 1.12; \quad INT_\psi = \frac{INT_\psi(ANLPD)}{INT_\psi(NLPD)} = 1.09$$

382 The plots of the adaption of the observer gains for the BS and NLPD  
 383 techniques are shown in Figs. 6 and 8, respectively. The estimation of the  
 384 disturbance made by the observer using the ABS and ANLPD, respectively,  
 385 is displayed at the bottom of Fig. 9.

386 **Remark 9.** *It is worth to note that in this manuscript, we have considered*  
 387 *constant disturbances on the real-time experiments to test the robustness of*  
 388 *the proposed controller. However, based on the results of Theorem 1, the*  
 389 *algorithm is robust towards bounded time-varying external disturbances the-*  
 390 *oretically. This scenario will be part of a future research in this topic.*

## 391 6. Conclusion

392 In this paper, an adaptive disturbance observer based on the extended  
 393 state observer and high order sliding mode technique has been proposed. The  
 394 adaptive disturbance observer is introduced into the Backstepping and non-  
 395 linear PD controllers to improve the performance of these techniques. The  
 396 stability analysis for the resulting closed-loop system for trajectory track-  
 397 ing has been addressed. The proposed controller has been implemented for  
 398 trajectory tracking in depth and yaw motions with the *Leonard* underwa-  
 399 ter vehicle and have been compared to the nominal design proposed in our  
 400 previous works. The real-time experiments results demonstrate the effective-  
 401 ness, robustness, and improvement of the proposed scheme to uncertainties  
 402 on the parameters of the system (damping and buoyancy changes) and to  
 403 external disturbances, as well. In this manuscript, constant disturbances  
 404 were considered, the robustness of the proposed towards time-varying exter-  
 405 nal disturbances and the improvement of the proposed scheme are part of  
 406 the future work.

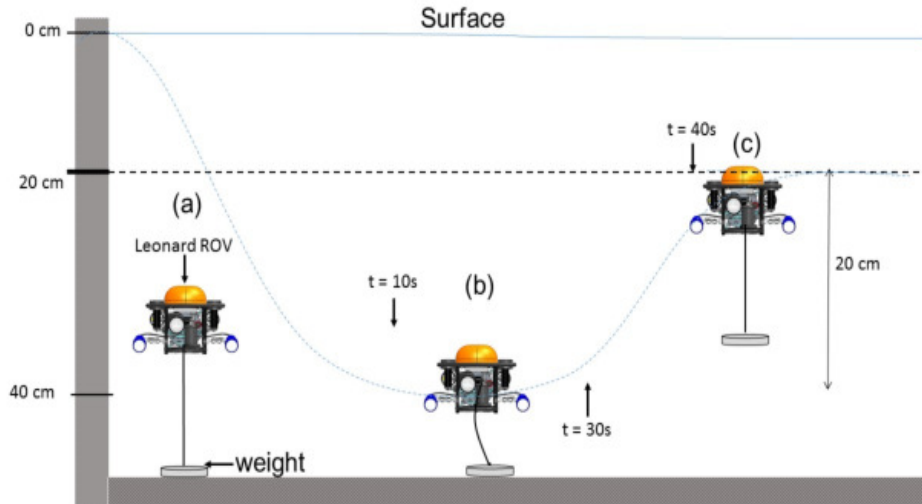


Figure 3: Description of the third scenario. (a) A  $1\text{ kg}$  load is attached to the Submarine. When the robot reaches  $30\text{ cm}$ , the influence of the weight disappears (b). Finally, the robot comes up again and the influence of the weight acts again on the robot (c).

#### 407 **Acknowledgment**

408 The authors would like to express their gratitude to the anonymous  
 409 reviewers for the comments to the improvement of the manuscript. The  
 410 Leonard underwater vehicle has been financed by the European Union (FEDER  
 411 grant n° 49793) and the Region Occitanie (ARPE Pilot Plus project). The  
 412 authors thank CONACYT for the scholarship grant (490978).

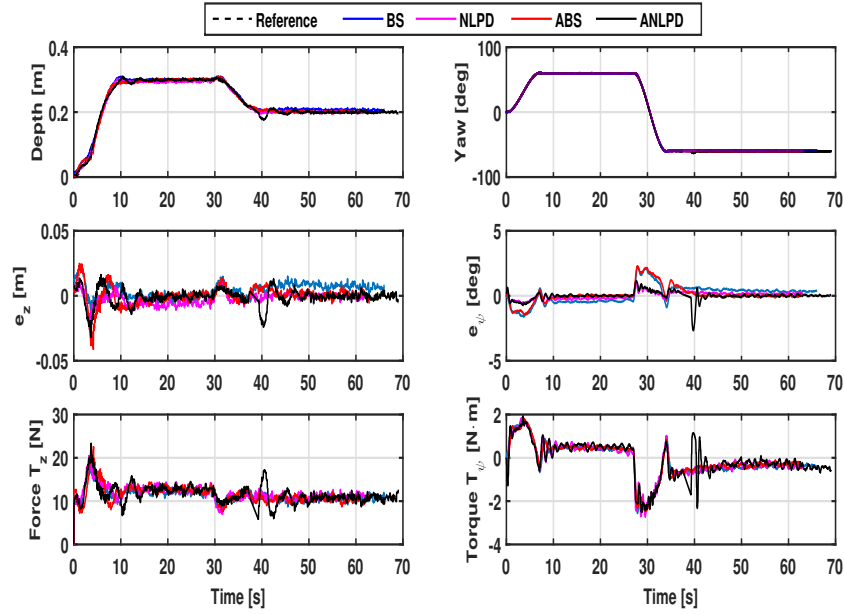


Figure 4: Performance of the NLPD and BS and their adaptive schemes for the depth and yaw tracking trajectory task in the nominal case.

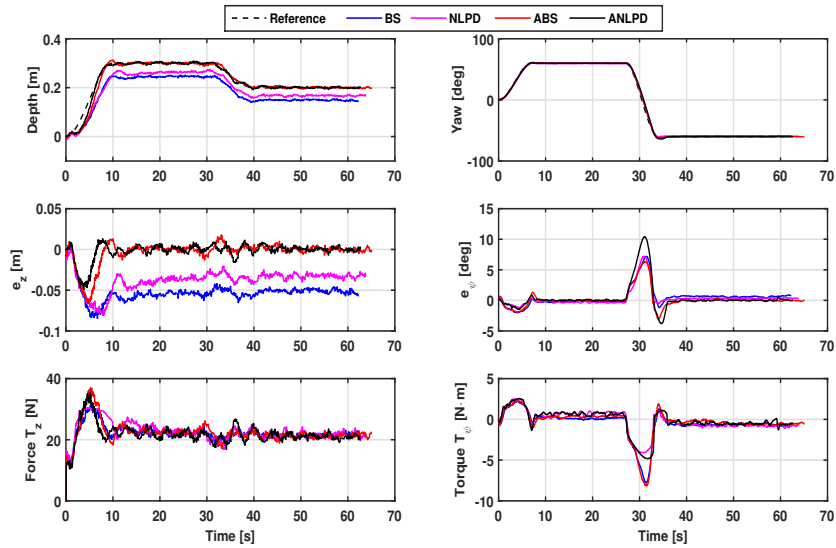


Figure 5: Robustness of the BS and NLPD and their adaptive versions behavior to parametric uncertainties. The floatability of the submarine was increased +100%, while the damping along z-axis was modify up to 90% with respect to the nominal case.

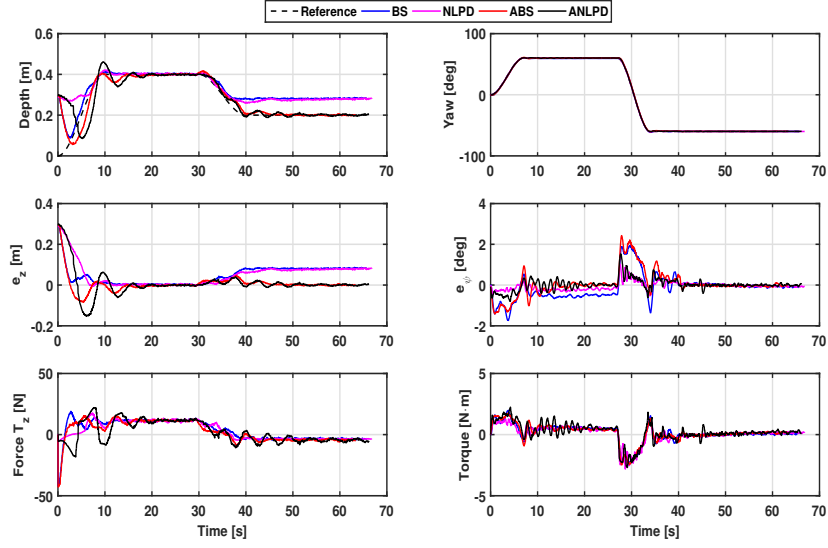


Figure 6: Robustness of the BS, ANLPD and their adaptive versions to external disturbances: Release and recovery of a load.

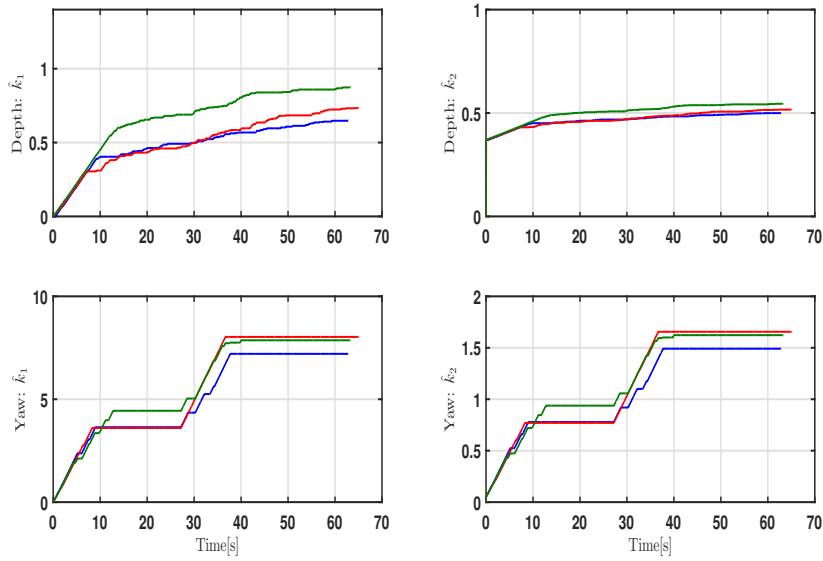


Figure 7: The dynamic gains evolution of the adaptive Backstepping disturbance observer: The nominal case (blue line), scenario 2 (red line) and scenario 3 (green line).

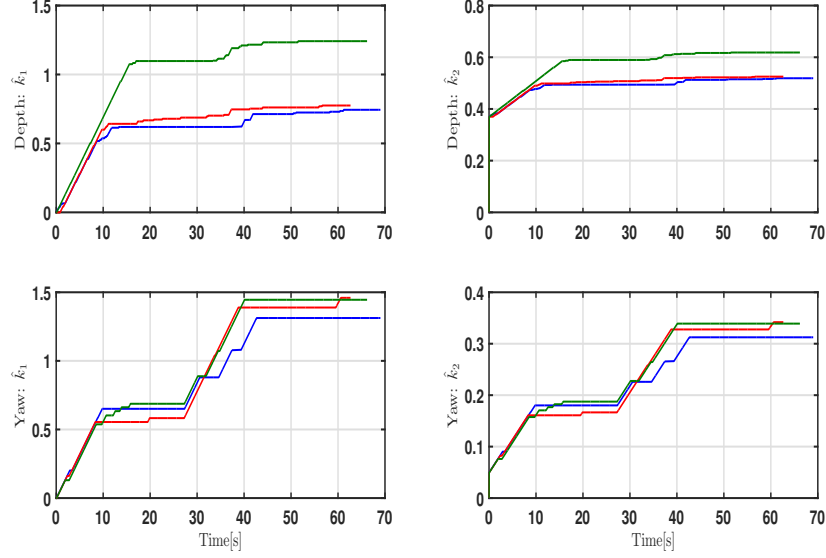


Figure 8: Evolution of the ANLPD disturbance observer gains: Nominal case (blue line), scenario 2 (red line) and scenario 3 (green line).

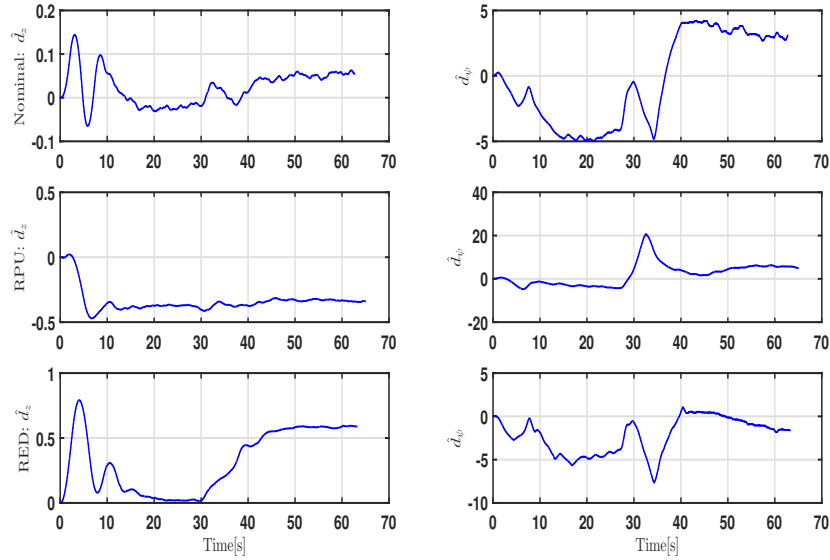


Figure 9: Disturbances estimated by the ABS: Nominal case (upper), robustness towards parametric uncertainties (middle) and robustness towards external disturbances (bottom).

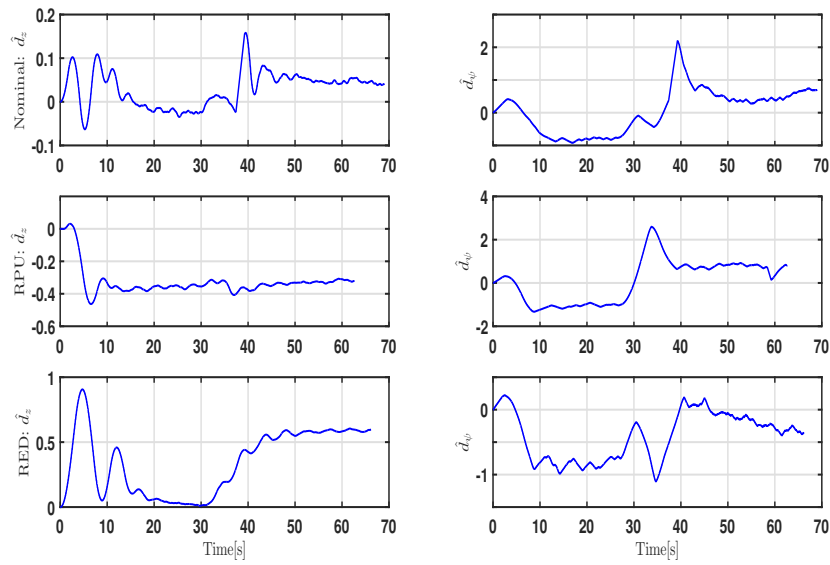


Figure 10: Disturbances estimated by the ANLPD: Nominal case (upper), robustness towards parametric uncertainties (middle) and robustness towards external disturbances (bottom).

Case	BS		ABS	
	$RMSE_z[m]$	$RMSE_\psi[deg]$	$RMSE_z[m]$	$RMSE_\psi[deg]$
Nominal	0.0043	0.1041	0.0001	0.1071
Parametric Uncertainties	0.0530	0.4891	0.0031	0.1487
External Disturbances	0.0476	0.1210	0.0053	0.0661

Table 5: Root Mean Square Error for BS and ABS design.

Case	NLPD		ANLPD	
	$RMSE_z[m]$	$RMSE_\psi[deg]$	$RMSE_z[m]$	$RMSE_\psi[deg]$
Nominal	0.0023	0.0265	0.0007	0.0099
Parametric Uncertainties	0.0374	0.3371	0.0018	0.4068
External Disturbances	0.0522	0.0571	0.0079	0.0170

Table 6: Root Mean Square Error for NLPD and ANLPD designs.

Case	BS		ABS	
	$INT_z$	$INT_\psi$	$INT_z$	$INT_\psi$
Nominal	546	33	557	28
Parametric Uncertainties	1064	48	1077	48
External Disturbances	373	28	361	27

Table 7: Integral control of inputs for BS and ABS designs.

<b>Case</b>	<b>NLPD</b>		<b>ANLPD</b>	
	$INT_z$	$INT_\psi$	$INT_z$	$INT_\psi$
Nominal	567	25	557	29
Parametric Uncertainties	1099	51	1054	52
External Disturbances	361	32	405	35

Table 8: Integral control of inputs for NLPD and ANLPD designs.

413 **References**

- 414 [1] S. Zhao, J. Yuh, Experimental study on advanced underwater robot  
415 control, *IEEE transactions on robotics* 21 (2005) 695–703.
- 416 [2] B. Jalving, The ndre-auv flight control system, *IEEE Journal of Oceanic*  
417 *Engineering* 19 (1994) 497–501.
- 418 [3] P. Herman, Decoupled pd set-point controller for underwater vehicles,  
419 *Ocean Engineering* 36 (2009) 529–534.
- 420 [4] T. I. Fossen, *Guidance and control of ocean vehicles*, John Wiley & Sons  
421 Inc, 1994.
- 422 [5] T. T. J. Prestero, Verification of a six-degree of freedom simulation  
423 model for the REMUS autonomous underwater vehicle, Ph.D. thesis,  
424 Massachusetts institute of technology, 2001.
- 425 [6] L. Moreira, C. G. Soares,  $H_2$  and  $H_\infty$  designs for diving and course  
426 control of an autonomous underwater vehicle in presence of waves, *IEEE*  
427 *Journal of Oceanic engineering* 33 (2008) 69–88.
- 428 [7] R. da Silva Tchilian, E. Rafikova, S. A. Gafurov, M. Rafikov, Optimal  
429 control of an underwater glider vehicle, *Procedia Engineering* 176 (2017)  
430 732–740.
- 431 [8] L. G. García-Valdovinos, T. Salgado-Jiménez, M. Bandala-Sánchez,  
432 L. Nava-Balanzar, R. Hernández-Alvarado, J. A. Cruz-Ledesma, Mod-  
433 elling, design and robust control of a remotely operated underwater ve-  
434 hicle, *International Journal of Advanced Robotic Systems* 11 (2014)  
435 1.
- 436 [9] Z. H. Ismail, V. W. Putranti, Second order sliding mode control scheme  
437 for an autonomous underwater vehicle with dynamic region concept,  
438 *Mathematical Problems in Engineering* 2015 (2015).
- 439 [10] J. Kim, H. Joe, S.-c. Yu, J. S. Lee, M. Kim, Time-delay controller  
440 design for position control of autonomous underwater vehicle under dis-  
441 turbances, *IEEE Transactions on Industrial Electronics* 63 (2016) 1052–  
442 1061.

- 443 [11] Y. Shtessel, M. Taleb, F. Plestan, A novel adaptive-gain supertwisting  
444 sliding mode controller: Methodology and application, *Automatica* 48  
445 (2012) 759–769.
- 446 [12] M. Krstic, I. Kanellakopoulos, P. V. Kokotovic, et al., *Nonlinear and*  
447 *adaptive control design*, volume 222, Wiley New York, 1995.
- 448 [13] B. Sun, D. Zhu, S. X. Yang, A bioinspired filtered backstepping tracking  
449 control of 7000-m manned submarine vehicle., *IEEE Trans. Industrial*  
450 *Electronics* 61 (2014) 3682–3693.
- 451 [14] J. Guerrero, J. Torres, E. Antonio, E. Campos, Autonomous underwa-  
452 ter vehicle robust path tracking: Generalized super-twisting algorithm  
453 and block backstepping controllers, *Journal of Control Engineering and*  
454 *Applied Informatics* 20 (2018) 51–63.
- 455 [15] L. Zhang, L. Zhang, S. Liu, J. Zhou, C. Papavassiliou, Low-level control  
456 technology of micro autonomous underwater vehicle based on intelligent  
457 computing, *Cluster Computing* (2018) 1–12.
- 458 [16] P. Sarhadi, A. R. Noei, A. Khosravi, Model reference adaptive pid  
459 control with anti-windup compensator for an autonomous underwater  
460 vehicle, *Robotics and Autonomous Systems* 83 (2016) 87–93.
- 461 [17] M. H. Khodayari, S. Balochian, Modeling and control of autonomous  
462 underwater vehicle (auv) in heading and depth attitude via self-adaptive  
463 fuzzy pid controller, *Journal of Marine Science and Technology* 20 (2015)  
464 559–578.
- 465 [18] E. Campos, A. Chemori, V. Creuze, J. Torres, R. Lozano, Saturation  
466 based nonlinear depth and yaw control of underwater vehicles with sta-  
467 bility analysis and real-time experiments, *Mechatronics* 45 (2017) 49–59.
- 468 [19] J. Guerrero, J. Torres, V. Creuze, A. Chemori, E. Campos, Saturation  
469 based nonlinear pid control for underwater vehicles: Design, stability  
470 analysis and experiments, *Mechatronics* 61 (2019) 96–105.
- 471 [20] R. Cui, L. Chen, C. Yang, M. Chen, Extended state observer-based  
472 integral sliding mode control for an underwater robot with unknown  
473 disturbances and uncertain nonlinearities, *IEEE Transactions on Indus-*  
474 *trial Electronics* 64 (2017) 6785–6795.

- 475 [21] J. A. Moreno, A linear framework for the robust stability analysis of a  
476 generalized super-twisting algorithm, in: Electrical Engineering, Com-  
477 puting Science and Automatic Control, CCE, 2009 6th International  
478 Conference on, IEEE, pp. 1–6.
- 479 [22] J. Guerrero, J. Torres, V. Creuze, A. Chemori, Trajectory tracking for  
480 autonomous underwater vehicle: An adaptive approach, *Ocean Engi-  
481 neering* 172 (2019) 511–522.
- 482 [23] S. of Naval Architects, M. E. U. Technical, R. C. H. Subcommittee,  
483 Nomenclature for Treating the Motion of a Submerged Body Through a  
484 Fluid: Report of the American Towing Tank Conference, Technical and  
485 research bulletin, Society of Naval Architects and Marine Engineers,  
486 1950.
- 487 [24] T. I. Fossen, *Marine control systems: guidance, navigation and control  
488 of ships, rigs and underwater vehicles*, 2002.
- 489 [25] J. C. Kinsey, R. M. Eustice, L. L. Whitcomb, A survey of underwater  
490 vehicle navigation: Recent advances and new challenges, in: IFAC Con-  
491 ference of Manoeuvring and Control of Marine Craft, volume 88, pp.  
492 1–12.
- 493 [26] S. Soyly, B. J. Buckham, R. P. Podhorodeski, A chattering-free sliding-  
494 mode controller for underwater vehicles with fault-tolerant infinity-norm  
495 thrust allocation, *Ocean Engineering* 35 (2008) 1647–1659.
- 496 [27] J. Han, A class of extended state observers for uncertain systems, *Con-  
497 trol and decision* 10 (1995) 85–88.
- 498 [28] J. Han, Auto-disturbance rejection control and its applications, *Control  
499 and decision* 13 (1998) 19–23.
- 500 [29] J. Guerrero, J. Torres, V. Creuze, A. Chemori, Observation-based non-  
501 linear proportional–derivative control for robust trajectory tracking for  
502 autonomous underwater vehicles, *IEEE Journal of Oceanic Engineering*  
503 (2019).
- 504 [30] F. Plestan, Y. Shtessel, V. Bregeault, A. Poznyak, New methodologies  
505 for adaptive sliding mode control, *International journal of control* 83  
506 (2010) 1907–1919.

- 507 [31] A. Levant, Sliding order and sliding accuracy in sliding mode control,  
508 International journal of control 58 (1993) 1247–1263.
- 509 [32] Y. Zhang, P. Yan, Sliding mode disturbance observer-based adaptive  
510 integral backstepping control of a piezoelectric nano-manipulator, Smart  
511 Materials and Structures 25 (2016) 125011.